Design and Characterization of the Interlayer Joint between Low-Field Nb_3Sn Conductors of a Layer Wound DEMO TF Coil

L. Muzzi, *Senior Member, IEEE*, L. Affinito, S. Chiarelli, V. Corato, A. della Corte, *Fellow, IEEE*, G. De Marzi, A. Di Zenobio, C. Fiamozzi Zignani, R. Freda, S. Turtù, *Senior Member, IEEE*, A. Anemona, A. Formichetti, R. Righetti, M. Arabi, A. Bragagni, M. Seri, G. Roveta, M. Roveta, S. Galignano, L. Merli, G. Molino, P. Bruzzone, M. Kumar, K. Sedlak, B. Stepanov

***Abstract*— In the frame of the conceptual design studies for the Toroidal Field (TF) coils of DEMO, a solution based on a layer-wound magnet, rectangular-shaped Cable-in-Conduit conductors and W&R manufacturing approach, is being developed. The feasibility and performance of a large-size Nb_3Sn conductor operating at about 82 kA in a 13 T field has been proven in the past. Another key technology to be demonstrated for a layer-wound TF coil, is that of a joint between two different conductor grades, to be possibly manufactured in-line during winding. The proposed joint solution would provide the minimum room occupancy, with the joint embedded within the winding pack volume. A joint between two low-field conductor grades, i.e. constituted of a small number of superconducting strands and a high number of stabilization copper wires, has been designed and manufactured. The two conductor lengths are characterized by a different number of superconducting wires and different outer dimensions. A joint sample has been assembled and instrumented, in the configuration allowing testing at the SULTAN facility of the Swiss Plasma Center. Both DC and AC performance of the joint has been characterized at the DEMO TF operating conditions. The present paper reports the main manufacturing steps for the joint and its main test results. The implications on the performance and design approach of the TF coil are also discussed, based on the outcome of such tests.**

***Index Terms*——Superconducting magnet, DEMO, Cable-in-Conduit-Conductor, Joint Resistance, AC loss, Fusion Magnets.**

I. Introduction

WITHIN the scope of the design studies for the project DEMO, the future European nuclear fusion reactor, coordinated by the EUROfusion consortium [1], one of the milestones is considered the feasibility demonstration of the large-current Nb_3Sn conductor solutions being proposed [2]. In particular, we refer here to the studies for the conductor of the Toroidal Field (TF) Magnet.

In 2016, the feasibility and performance of a Cable-in-Conduit Conductor (CICC) characterized by a rectangular geometry, low void fraction (VF) and distributed pressure relief channels, has been successfully demonstrated [3]. The solution for the TF coil being investigated by ENEA is that of a Wind & React (WR), layer-wound coil, and the tested conductor was designed to fulfil the requirements of the high field (HF) grade within the winding pack (WP). That CICC demonstrated performance with stable operation up to 81.7 kA and a magnetic field of 13 T. Successful results were also achieved by the advanced development at the Swiss Plasma Center (SPC) of a HF CICC based on a flat cable layout, with mixed-matrix stabilizer and React & Wind (RW) manufacturing approach [4].

The design, manufacture and performance verification of low field (LF) CICC types, characterized by a small fraction of superconductor with respect to that of the stabilizing copper, as well as of inter-layer joints between conductors of different grades, are considered additional fundamental steps for qualification of a layer-wound coil concept. Conductor lengths representative of the two lowest field grade CICCs within the WR TF coil design, characterized by a different number of superconducting and stabilizing copper wires, by different jacket thickness and by different outer dimensions, have been manufactured. A joint between the two LF CICC has been designed and manufactured, as well. It follows the "invisible", butt joint design approach, originally developed at ENEA [5] and adopted in other projects [6, 7, 8], characterized by a low resistance and outer dimensions equal or slightly larger than those of the constituting CICCs. In order to qualify its design, a sample has been assembled and tested in the SULTAN facility at SPC. The present paper reports a detailed description of the CICCs and of the joint sample manufacture, with its main test results.

L. Muzzi, L. Affinito, S. Chiarelli, V. Corato, A. della Corte, G. De Marzi, A. Di Zenobio, C. Fiamozzi Zignani, R. Freda, S. Turtù are with ENEA, Via E. Fermi 45, Frascati, I-00044, Italy (e-mail: luigi.muzzi@enea.it).

A. Anemona, A. Formichetti, R. Righetti are with ICAS Srl, Frascati, Italy.

A. Bragagni, M. Seri, M. Arabi are with TRATOS Cavi SpA, Pieve Santo Stefano, Italy.

G. Roveta, M. Roveta, S. Galignano, L. Merli and G. Molino are with CRIOTEC Impianti SpA, Chivasso, Italy.

P. Bruzzone, M. Kumar, K. Sedlak, B. Stepanov, with École Polytechnique Fédérale de Lausanne (EPFL), Swiss Plasma Center (SPC), CH-5232 Villigen PSI, Switzerland.

Color versions of one or more of the figures in this paper are available online at http://ieeexplore.ieee.org.

Digital Object Identifier will be inserted here upon acceptance.

II. Low-Field Rectangular CICCs

A. The Strands

The superconducting wires supplied by the Chinese Company Western Superconducting Technologies (WST), were characterized by a diameter of 1.0 mm, a Cu:nonCu = 1, and a critical current density: J_{c_nonCu}(4.2K, 12T, 0%) > 950 A/mm^2. The cables include both 1.0 mm and 1.5 mm diameter Cr-coated Cu wires, with residual resistivity ratio (after heat treatment): $RRR_{273K/20K}$ > 300. WST and Luvata supplied the 1.0 mm and 1.5 mm Cu wires, respectively.

Measurements carried out after heat treatment with 200 hours duration at the 650 °C plateau are: critical current (I_c) on standard ITER barrel in liquid helium, that confirmed values for different billets in the range 370 A ÷ 395 A; AC hysteretic losses by Vibrating Sample Magnetometer (VSM), to determine hysteresis losses, Q_{hyst}, and, by comparison with transport data, the wire effective filament diameter, d_{eff}. As a result, Q_{hyst} = 790 mJ/cm^3, measured over a ±3T cycle at 0.5 T/min. and referred to the entire wire volume; d_{eff} = 34 μm.

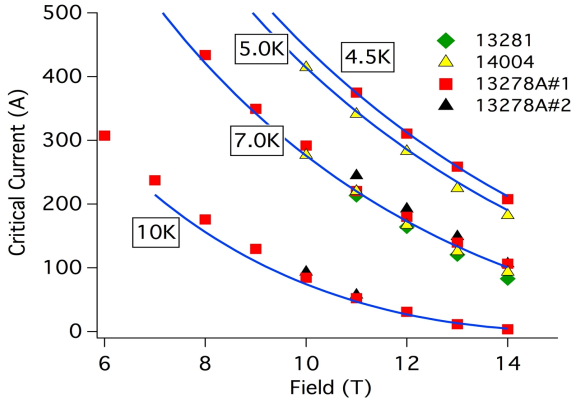

Fig. 1. I_c measured as function of field with the ENEA Walters spring system [12] at zero applied strain, with the wire soldered to the CuBe holder, and at different temperatures. Symbols are measured data on samples from different billets. Continuous lines are fits using the ITER scaling law [13] with the parameter set of Table I.

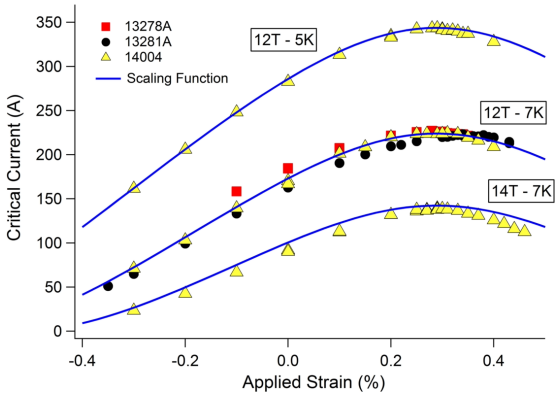

Fig. 2. I_c measured as function of applied strain at different field – temperature conditions, and on samples from different billets. Symbols are measured data. Continuous lines are fits using the ITER scaling law [13] with the parameter set of Table I.

In addition, since the Nb_3Sn wires operate in CICCs under strain [9, 10, 11], we also carried out a complete characterization of the wires with the ENEA Walters Spring (WASP) test facility [12], thus in terms of critical current as function of applied axial strain, ε_{ax}, applied magnetic field, and temperature. This allows reconstructing reliably the I_c performance over a wide strain–temperature–field range, based on the ITER scaling law formulation [13]. Figs. 1 and 2 show a summary of measured results, as compared to a fit carried out using the parameter set reported in Table I.

TABLE I
Scaling Parameters of the 1.0mm WST Nb_3Sn Strands According to the ITER Scaling Relation [13]

Parameter	Value
C_{a1}	53.00
C_{a2}	0.000
$\varepsilon_{0,a}$, [%]	0.312%
ε_m, [%]	-0.289%
$\mu_0 H_{c2m}(0)$, [T]	33.24
$T_{cm}(0)$, [K]	16.34
C_1, [AT]	30401
p	0.593
Q	2.156

B. The CICCs

The conductor designed by ENEA for the DEMO TF magnet is a rectangular CICC, obtained through lamination of a round steel tube after insertion of the cable. The cable has 6 "petals", each covered for 50% by steel wrapping. Three of them are made of elements cabled around a central steel spiral. The cable has a central Cu core, and is wrapped with an overlapped steel tape. The CICCs WR2 and WR3 were designed to operate at 70.8 kA and at 7.1 T and 6.0 T, respectively. Therefore, they contain a different number of superconducting wires, and are characterized by a different non-Cu current density, $J_{non\text{-}Cu}$. Table II summarizes their main features.

TABLE II
Main Parameters of the DEMO TF WR2 and WR3 CICCs

Parameter	CICC #1 – WR2	CICC #2 – WR3
Operating Current, I_{op}	70.8 kA	
Effective field, B_{eff}	7.1 T	6.0 T
Numb. SC strands	180	120
SC strand diam.	1.0 mm	
Numb. Cu strands (1.0 mm / 1.5 mm)	630 / 108	690 / 108
Non-Cu current density	$J_{non\text{-}Cu}$=1002 A/mm^2	$J_{non\text{-}Cu}$=1502 A/mm^2
Cu current density (at quench)	J_{Cu}=93.6 A/mm^2	J_{Cu}=90.8 A/mm^2
Cable layout: S1	$S1_a$ = 1 s.c. + 2 Cu; $S1_b$ = 3 Cu	
Cable layout: S2 & S3	(2 x $S1_a$ + $S1_b$)x3	[(2 x $S1_a$ + $S1_b$)x2 + $S1_b$ x3]
Cable layout: S4	S3 x (5+C1) $S4_a$: C1 = 3 Cu x 4 (with 1.5 mm Cu wires) $S4_b$: C1 = steel spiral (with 7.0 mm outer dia.)	
Final cable layout	(3 x $S4_a$ + 3 x $S4_b$) around core C2 C2: 3 Cu x 4 x 6 (with 1.5 mm Cu wires)	
Cable twist pitches	110/125/145/175/500 mm (core C1: 110 / 170; core C2: 110 / 170 / 245)	
CICC external dim.	36.6 x 64.4 mm^2	44.9 x 70.7 mm^2
Jacket thickness	5.5 mm	9.5 mm
V.F. in cable bundle	28.9%	28.3%

All cabling activities have been carried out by the company TRATOS Cavi, and all jacketing activities by CRIOTEC Impianti, using the ITER / JT-60SA CICC production lines [14].

Steel jackets suitable to attain final conductor dimensions were chosen, with the condition to have a sufficiently thick tube (> 5 mm) in order to be relevant for the proposed coil design. In particular, tubes with 5.5 mm x 60.3 mm (thickness x outer diameter) and 9.5 mm x 73.0 mm were chosen. The final CICC outer dimensions (see Table II) were chosen to attain the target 26% void fraction in cable bundle.

The manufacturing activities have provided very important feed-backs for similar LF CICC designs, in the following terms: the cooling spirals within the petals should sustain the compaction required to obtain low VF values (about 26% or less). It was demonstrated in the past with a similar CICC design [3] that a spiral made of a 1 mm thick strip was able to sustain this pressure. Here, we were only able to procure a steel spiral made of a thin (0.5 mm, instead of the nominal 1.0 mm) strip, thus very easily deformable, and unable to sustain the compaction without squeezing. Alternatively, a design with larger spiral, occupying the cross-section of a cable petal, as developed in the frame of the Korean DEMO project [15], should be explored. Finally, for LF rectangular CICC geometries, a large cable central core causes an excessive deformation of the petals in the regions close to the middle of the large conductor face. The corresponding segregated Cu cross-section could be added more effectively at the last cabling stage within the interstices between adjacent petals.

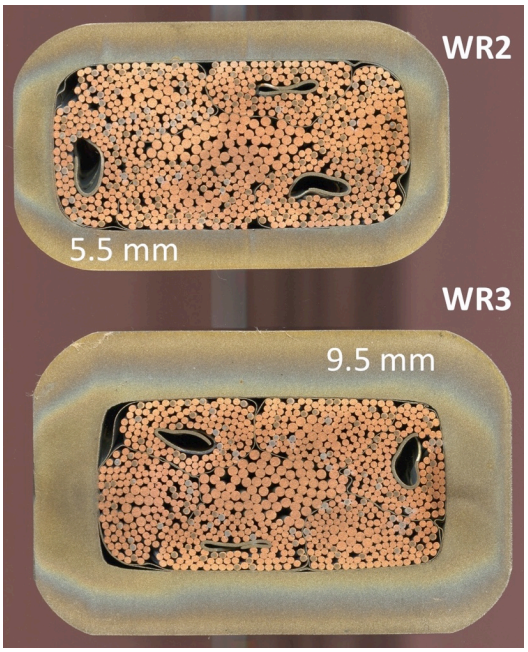

Fig. 3. Cross-section cut by electro-erosion of the two WR2 and WR3 CICC samples. The small number of superconducting wires in cross-section is evident, as well as the unwanted squeezing of the thin cooling channels.

Anyhow, the round-to-rectangular compaction of large conductors with thick steel jackets doesn't present relevant issues. A cut by electro-erosion of each of the two CICC types has been carried out, as shown in Fig. 3. From this, the local void fraction in cable bundles (excluding the spiral area) has been estimated by image analysis: it is 28.9% for WR2, and 28.3% for WR3. As expected, the spiral collapse determines a larger local VF with respect to the target design value of 26%.

III. Inter-layer Joint

A. Joint Concept and Design

Main aim of the present work was to study the feasibility of the inter-layer joints connecting the different Double Layers within the DEMO TF Winding Pack, each made of Nb_3Sn rectangular conductors with different superconducting cross-section and steel thickness, according to the specific electromagnetic and mechanical requirements.

The location of the inter-layer joints on the outboard leg of the D-shaped winding pack determines its operating conditions. A preliminary assessment of its possible positioning has been performed by evaluating the magnetic field distribution, at the End-of-Burn (EOB) instant of the plasma scenario. Different possible locations for the LF inter-layer joints have been identified, with magnetic fields between 2 T and 3 T, for example underneath the Poloidal Field coil 4 or 5.

As for the joint concept, the two cable ends to be joined are cut with a staggered geometry, so that the coupling of the two ends leads to a reconstruction of the original cable shape, including petal twisting. A Cu sleeve, either a U-shaped profile in which the reconstructed cable is laid down, or a tube large enough to pass over one of the CICC ends during ends preparation, is crimped around the cable, leaving a local void fraction below 15%. This Cu sleeve normally contributes to the current transfer between the two joined conductors. Properly shaped steel clamps enclose the joint and are welded to the steel jackets at the two conductor ends. The refrigerating fluid flows through grooves machined on the inner side of the steel sleeves. This kind of joint can in principle be manufactured in-line during winding, between the end of a layer winding, and the start of the following one. It could be mostly embedded within the winding pack volume, with only the He outlet pipes protruding outside of the assembly.

B. Joint Sample Manufacture

As layout of the SULTAN sample, one of the two legs (the RIGHT one) is made of the Low Field CICC WR2, which is then bent in a hairpin-type configuration. On the second Leg, the joint between WR2 and WR3 is manufactured, centered on the SULTAN background field location.

The various steps for the manufacture of the joint were (see Fig. 4): a) removal of the outer cable wrapping and of the spirals; b) chemical etching of the wires Cr coating; c) cut of the two cable ends to be joined, with a staggered geometry on the corresponding petals; d) cold-welding wire by wire of the central Cu core, and reconstruction of the cable geometry, with twisted petals; e) crimping of a copper tube over the joint region, that constitutes an additional path for the current transfer between the two conductor ends; f) lamination of the copper sleeve to its final rectangular geometry and dimensions to guarantee a low VF in the joint region below 15%; g) enclosure of the joint region inside the two pre-shaped steel halves, with dimensions on the two ends matching the corresponding jacket geometries, and internal grooves for Helium circulation; h) closure welding of the steel box, avoiding full penetration and controlling the heating of the superconducting wires; i) as-

sembly of the sample in a hairpin configuration, with manufacturing steps described with some details in [3].

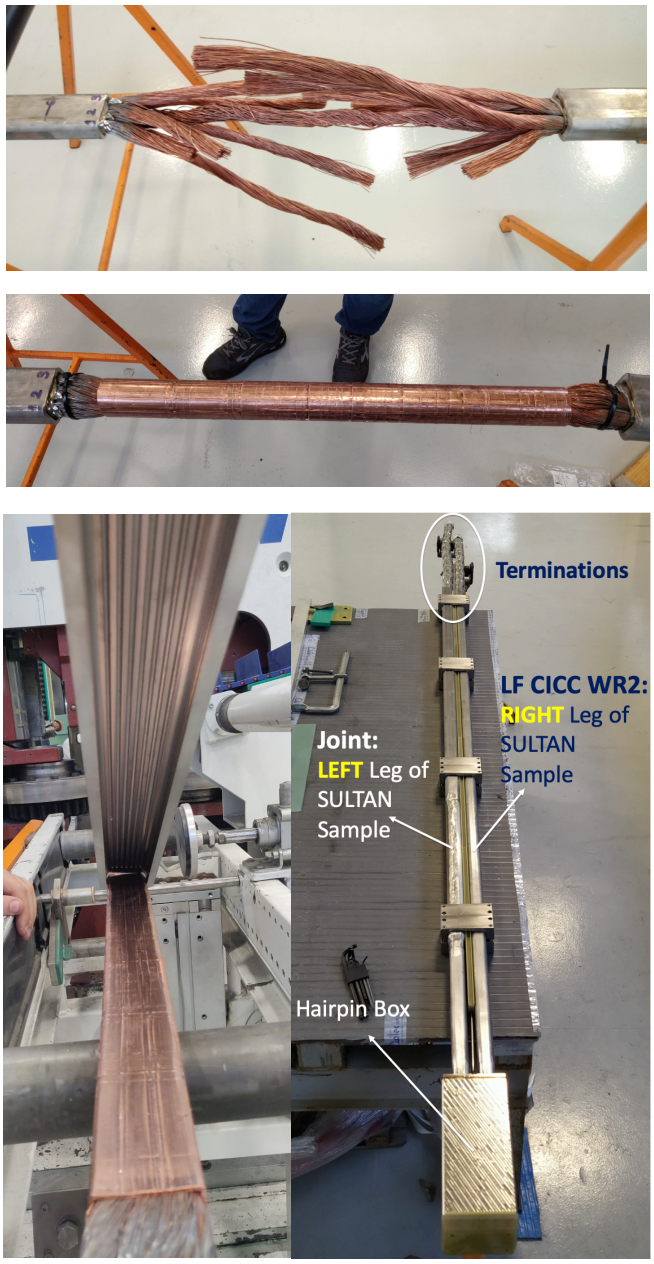

Fig. 4. Some pictures of the main manufacturing steps for the inter-layer joint. From top to bottom: the two cable ends after Cr-coating removal and cut with staggered geometry; crimping of the Cu sleeve; lamination to the final geometry and dimensions; closing of steel box with grooves for He circulation (left); final joint sample (right), after assembly of the bottom hairpin box.

All successive manufacturing steps have been performed at SPC. The two upper terminations were realized by crimping a Cu sleeve around the cable bundle, after removal of the cable wrapping and of the Chromium coating. The sleeve was prepared with a transition piece to steel, for the welding to the CICC jacket. After the Nb_3Sn reaction heat treatment, the terminations were dipped in solder bath and soldered inside pre-tinned slots of rectangular copper plates.

Instrumentation for both sample legs includes voltage taps across the SULTAN high field zone, with a set enclosing the joint over its 690 mm extension, another one installed over a longer length, of 1090 mm. Up to six voltage taps are attached on the same CICC cross-section, on different sides. Temperature sensors are attached to the jacket, both upstream and downstream of the joint position, with two sensors monitoring the temperature at each position, over the long CICC sides.

IV. SULTAN Test

The testing program was defined with the aim of characterizing the inter-layer joint at different magnetic field (up to 9 T) and transport current (up to the nominal I_{op}: 70.8 kA), before and after 570 electromagnetic cycles performed at 6 T and 55 kA, followed by a warm-up and cool-down (WUCD) cycle. AC losses have been measured on both the joint and the CICC constituting the second sample leg, with both sinusoidal and trapezoidal AC varying fields. Stability runs have also been carried out after cycling, at 6 T background field and 50 kA transport current. The main test results are reported in the following sections. For comparison, expected performance of the two CICCs, are reported in Table III, as computed considering the strand scaling law (see Table II), and an effective operating strain of -0.55%, as determined on the High-Field CICC, having the same layout [3].

TABLE III
Expected Critical Current of the Two Low Field CICCs constituting the Inter-Layer Joint, at Relevant Conditions for the Present Tests

Parameter	Value					
Operating conditions	4 T; 5 K		6 T; 5 K		8 T; 5 K	
CICC type	WR3	WR2	WR3	WR2	WR3	WR2
Critical current (kA)	125	187	81	122	54	81

A. Joint Resistance tests

The complete set of DC measurements carried at different SULTAN background field and transport current, both before and after cycling, and determined using different voltage tap pairs, are reported in Figs. 5 and 6. Up to about 2 T of background field, the joint resistance is below 0.5 nΩ, and up to about 4.5 T, it remains below about 1.0 nΩ up to 70.8 kA. At higher fields, saturation of the superconductor occurs, and the joint resistance increases. Above 4.5 T, quenches are observed before reaching the nominal 70.8 kA. By comparing the results with the expected CICC performance (see Table III), it appears that in this joint configuration, with each cut petal relying on local current transfer to neighboring petals, to the central Cu core, and to the outer sleeve, the superconductor saturates at about half of the critical current of the CICC WR3. Then, current redistributes from lower to higher resistivity paths. The large unbalance between Cu and superconducting strands might play a key role for the performance of this joint, and a possible improvement could be to keep all superconducting wires intact all along the entire joint length, thus reducing the effective inter-strand resistance. It should also be observed that the outer Cu sleeve was chosen with low RRR, to limit AC losses, and it most likely represents the high resistance parallel current path at increasing superconductor saturation. Finally, it cannot be excluded that the strong compaction below the Cu sleeve may have damaged part of the al-

ready few superconducting wires; this will need to be investigated in detail by destructive metallographic analyses.

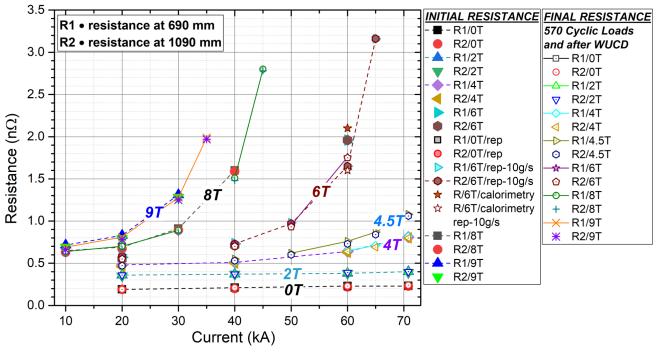

Fig. 5. DC measurements of joint resistance as function of the sample transport current, at different background magnetic fields, before (closed symbols) and after (open symbols) loading and thermal cycles.

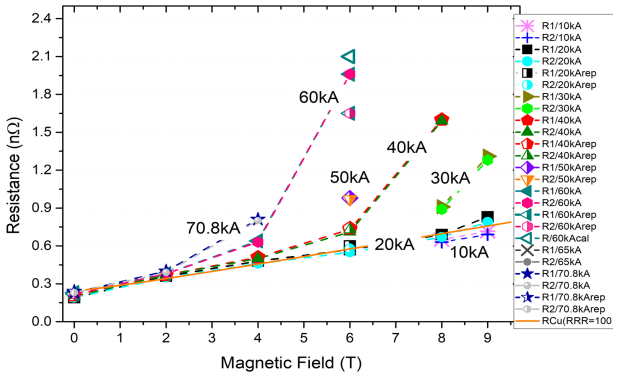

Fig. 6. DC measurements of joint resistance as function of the background field, at different currents. Before joint saturation, the measurements are well described by a Cu with RRR = 100 (thick orange line in figure).

B. *AC losses tests – sinusoidal cycles*

AC losses on the virgin sample are measured with sinusoidal cycles with varying frequency up to 1 Hz and AC field amplitude B_{ac} = ± 0.3 T, applied perpendicularly to the wide conductor surface, and at background field of 2 T. After cycling, additional AC losses are measured with 6 T background field, and with a sample current of 50 kA. AC losses are determined calorimetrically, evaluating the temperature variation at the measured helium mass flow rate, for each of the two legs. The main results are reported in Figs. 7 and 8.

AC losses of the joint are characterized by a peak at frequencies below 0.1 Hz. This behavior was observed also on the ITER TF joint, and on a first prototype of the inter-layer joint for the DEMO HF RW CICC [16] that was however characterized by higher resistance. The same shape was also observed on some rectangular CICCs characterized by low Void Fraction and absence of petal wraps [3, 17, 18]. On the other hand, the LF CICC tested here, with wrapped petals (with 50% coverage), has the peak of losses at around 0.6 Hz in virgin conditions, that shifts to a frequency higher than 1 Hz after cycling. The role of coupling losses between the high cable stages (petal-to-petal), characterized by high time constant values (of the order of tens of seconds) seems to play the fundamental role in the very low frequency range. From the quantitative point of view, in the explored range AC losses of the joint are lower than those measured on the ITER TF and CS Twin-Box joints [16], as well as of those of the updated DEMO HF RW inter-layer joint [19], that had a very similar joint resistance. In addition, it can be observed that the results for the joint are practically unchanged with cycling, denoting a mechanically stable configuration. On the other hand, the LF CICC shows losses that decrease appreciably after cycling, denoting the expected increase of transverse resistances [17].

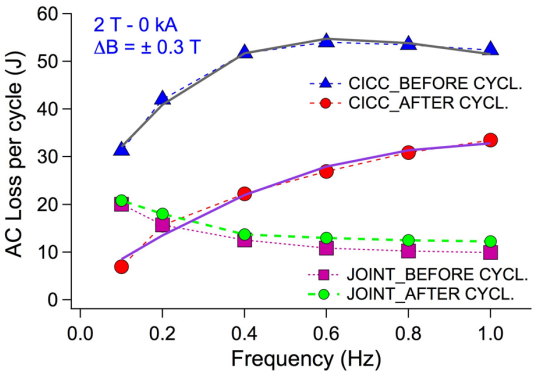

Fig. 7. AC losses measured under a sinusoidal varying field, as function of frequency, for both the joint and the CICC, before and after cycling. Thick solid lines are fits using a single time constant approximation, with $n\tau$ = 500 ms and 280 ms before and after cycling, respectively.

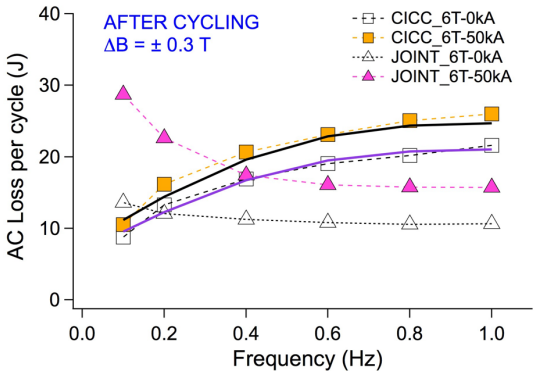

Fig. 8. AC losses measured under a sinusoidal varying field, as function of frequency, for both the joint and the CICC, at different background fields, and with or without 50 kA transport current. Thick solid lines are fits using a single time constant approximation, with $n\tau$ = 320 ms for both cases.

Fig. 8 reports the results measured with a background field of 6 T, with or without 50 kA of transport current, I_t. As expected, the AC losses decrease both for the joint and for the CICC, with respect to those measured at 2 T. However, at fixed field (i.e. 6 T), a dynamic resistance effect sets in, and the transport current contributes to the dissipation, leading to an increase of losses, especially evident for the joint in the very low frequency range.

For a correct interpretation of the measured AC losses, it should be considered that in multi-stage CICCs, the different transverse resistance of the cable stages results in multiple time constants [20, 21], determined by the multiple induced currents loops. Each time constant is relevant for a specific frequency range, and in general several time constants are needed in order to fit the Q *vs.* ω curve. When a transient AC

loss regime is dominant over the others, a single time constant is sufficient to describe the experimental data. As shown in Figs. 8 and 9, a satisfactory result is obtained here analyzing the CICC AC losses data with a single time constant approximation: at 2 T, a $n\tau$ = 500 ms is obtained, that reduces to $n\tau$ = 280 ms after applying cycles. Moreover, this does not change appreciably with increasing field, since all CICC data at 6 T of Fig. 8 are well described with a $n\tau$ = 320 ms. However, the peak shift after cycling towards frequencies higher than 1 Hz increases considerably the uncertainty in the determination of $n\tau$. Interestingly, the CICC AC loss with 50 kA (see Fig. 8) perfectly scales by a factor $[1+(I_t/I_c)^2]$ with respect to those at I_t = 0, as foreseen by most AC losses models [22].

Considering the joint, the data cannot be described with a simplified single time constant approximation, but the dominant time constant is higher than that of the conductor, as the peak lies below the lower measured frequency. This occurs because the transverse resistances in the joint are much lower than those of the CICC.

C. AC losses tests – trapezoidal runs

For a full characterization, also a series of unipolar trapezoidal pulsing 0 T - 0.3 T – 0 T was performed after cyclic loading, with 6 T background field and at different *dB/dt*, to define the effective coupling time constant ($n\tau$) of conductors, according to the procedure proposed in [23]. In terms of variation rates, these runs allow exploring the low frequency range (for example: the *dB/dt* with 4 sec ramp-up time corresponds to the peak variation rate of sinusoidal cycles at 0.04 Hz). In this range, as Fig. 9 shows, the effective coupling time constant of the CICC is smaller than the corresponding value measured on the joint, in agreement with what discussed in Section IV.B, and with the observation that joint AC losses measured with sinusoidal variations are higher than those of the CICC below about 0.2 Hz (cfr. Figs. 7 and 8).

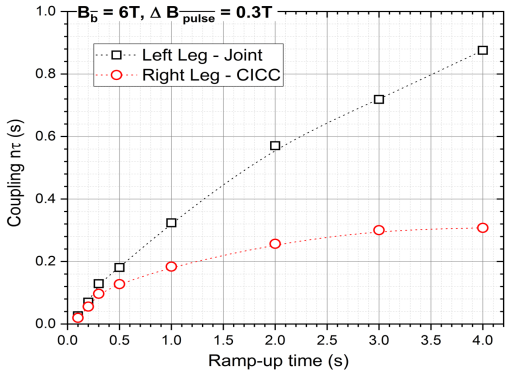

Fig. 9. Effective coupling time constant for the inter-layer joint (Left Leg – black square symbols), and for the CICC (Right Leg – red round symbols) as function of the ramp-up time with trapezoidal AC varying fields.

D. Stability tests

As a last item of the experimental campaign, Minimum Quench Energy (MQE) tests has been were performed, at 6 T background field, with sample current of 50 kA and helium mass flow rate 3 g/s. Full Sinusoidal pulses of 128 ms durations with varying amplitudes (up to 600 V maximum) were applied with the help of capacitor bank. Quench was only observed on the joint at 450 V, corresponding to a peak magnetic field variation of 18 T/s, and an energy deposition of about 100 Joule. The quench dynamics at this field variation rate clearly shows a voltage take-off at the joint and the effect of the discharge on the conductor temperature, which increases of about 3.5 K.

V. Conclusion

An inter-layer joint sample between two Low Field (LF), rectangular CICCs for the European DEMO TF Coil has been designed and manufactured. Reaction heat treatment, instrumentation installation and experimental tests have been carried out in SULTAN, at the Swiss Plasma Center.

The joint shows excellent DC performance for fields up to 2 T, with a resistance at 70.8 kA below 0.5 nΩ, and which remains below 1 nΩ up to about 4.5 T. At higher fields, the superconductor saturates, current redistributes through higher resistivity paths, as for example the low RRR Cu sleeve, and the joint resistance increases. Above 4.5 T, quench phenomena occur before reaching the target operating current (70.8 kA). The large unbalance between superconductor and copper fractions in the cables plays a major role, and calls for an improvement of the joint design, by using a lower resistivity and thicker Cu sleeve, or by choosing a different architecture of the petal cuts, preserving the integrity of the superconducting wires all along the joint length. Metallographic investigations will need to be carried out, to evidence possible damage of the already few superconducting strands in the joint region.

This joint is mechanically very stable, since no effect is observed on either joint resistance or AC losses, with electromagnetic and thermal cycling (570 Cycles at 6 T x 55 kA + warm-up / cool-down cycle).

The joint has very limited AC losses, with a peak at frequencies lower than 0.1 Hz. The low-field CICC has higher losses, peaking at about 0.6 Hz, and that reduce appreciably with cycling, while shifting the peak to frequencies higher than 1 Hz. In the explored range, the CICC losses can be satisfactorily described using a single time constant model, with a value $n\tau$ = 280 ms for the CICC after cycling.

The joint stability has been explored with full sinusoidal AC pulses of 128 ms durations with varying amplitudes, and with 50 kA of current, and it is very stable up to a peak magnetic field variation rate of 18 T/s.

Acknowledgment

This work has been carried out within the framework of the EUROfusion Consortium and has received funding from the Euratom research and training programme 2014-2018 and 2019-2020 under grant agreement No 633053. The views and opinions expressed herein do not necessarily reflect those of the European Commission.

REFERENCES

[1] G. Federici *et al.*, "Overview of the design approach and prioritization of R&D activities towards an EU DEMO", *Fus. Eng. Des.*, vols. 109-111, Part B, pp. 1464-1474, Nov. 2016.

[2] K. Sedlak *et al.*, "Advance in the conceptual design of the European DEMO magnet system", *Supercond. Sci. Technol.*, vol. 33, 2020, Art. ID. 044013.

[3] L. Muzzi *et al.*, "Design, Manufacture, and Test of an 80 kA-Class Nb_3Sn Cable-in-Conduit Conductor with Rectangular Geometry and Distirbuted Pressure Relief Channels", *IEEE Trans. On Appl. Supercond.*, vol. 27, no. 4, 2017, Art. ID. 4800206.

[4] K. Sedlak *et al.*, "DC Test Results of the DEMO TF React&Wind Conductor Prototype No. 2", *IEEE Trans. On Appl. Supercond.*, vol. 29, no. 5, 2019, Art. ID. 4801005.

[5] A. Di Zenobio *et al.*, "Joint Design for the EDIPO", *IEEE Trans. On Appl. Supercond.*, vol. 18, no. 2, 2008, p. 192.

[6] A. Portone *et al.*, "Design and Procurement of the European Dipole (EDIPO) Superconducting Magnet", *IEEE Trans. On Appl. Supercond.*, vol. 18, no. 2, 2008, p. 499.

[7] V. Corato *et al.*, "Detailed design of the large-bore 8 T superconducting magnet for the NAFASSY test facility", *Supercond. Sci. Technol.*, vol. 28, 2015, Art. ID. 034005.

[8] N. Martovetsky *et al.*, "Development of the Joints for ITER Central Solenoid", *IEEE Trans. On Appl. Supercond.*, vol. 21, no. 3, 2011, p. 1922.

[9] D. Uglietti, K. Sedlak, R. Wesche, P. Bruzzone, L. Muzzi, and A. della Corte, "Progressing in cable-in-conduit for fusion magnets: from ITER to low cost, high performance DEMO", *Supercond. Sci. Technol.*, vol. 31, 2018, Art. ID. 055004.

[10] L. Muzzi, G. De Marzi, A. Di Zenobio and A. della Corte, "Cable-In-Conduit Conductors: lessons from the recent past for future developments with low and high temperature superconductors", *Supercond. Sci. Technol.*, vol. 28, 2015, Art. ID. 053001.

[11] A. Nijhuis and Y. Ilyin, "Transverse load optimization in Nb_3Sn CICC design; influence of cabling, void fraction and strand stiffness", *Supercond. Sci. Technol.*, vol. 19, 2006, pp. 945-962.

[12] L. Muzzi *et al.*, "E-WASP, a facility to test strain, temperature, magnetic field and current effects on superconducting samples", presented at the EUCAS2017 Conference, Sept. 2017. Available online at: https://indico.cern.ch/event/659554/timetable/

[13] L. Bottura, B. Bordini, "$J_c(B,T,\varepsilon)$ Parameterization for the ITER Nb_3Sn Production", *IEEE Trans. On Appl. Supercond.*, vol. 19, no. 3, 2009, pp. 1521-1524.

[14] A. della Corte *et al.*, "ITER and JT-60SA Conductor Production at ICAS", *IEEE Trans. On Appl. Supercond.*, vol. 23, no. 3, 2013, Art. ID. 4200904.

[15] K. Kim *et al.,* "Design concept of K-DEMO for near-term implementation", *Nucl. Fusion,* vol. 55, 2015, Art. ID. 053027.

[16] B. Stepanov *et al.*, "Inter-layer Joint for the TF Coils of DEMO – Design and Test Results", *IEEE Trans. On Appl. Supercond.*, vol. 28, no. 3, 2018, Art. ID. 4201104.

[17] K. Yagotintsev and A. Nijhuis, "AC loss, interstrand resistance and mechanical properties of prototype EU DEMO TF conductors up to 30000 load cycles", *Supercond. Sci. Technol.*, vol. 31, 2018, Art. ID. 025010.

[18] K. Sedlak *et al.*, "Test of the MF-CICC Conductor Designed for the 12 T Outsert Coil of the HFML 45 T Hybrid Magnet", *IEEE Trans. On Appl. Supercond.*, vol. 26, no. 4, 2016, Art. ID. 4300305.

[19] V. D'Auria *et al.*, "Inter-layer Joint of Nb_3Sn React&Wind Cables for Fusion Magnets", *IEEE Trans. On Appl. Supercond.*, vol. 30, no. 4, 2020, Art. ID. 4200505.

[20] A. Nijhuis, H. H. J. ten Kate, J. L. Duchateau, P. Bruzzone, "Coupling Loss Time Constants in Full-Size Nb_3Sn CIC Model Conductors for Fusion Magnets," *Adv. Cryo. Eng. Mat.*, vol. 42, 1996, pp. 1281-1288.

[21] B. Turck, L. Zani, "A macroscopic model for coupling current losses in cables made of multistages of superconducting strands and its experimental validation," *Cryogenics*, vol. 50, 2010, pp. 443-449.

[22] T. Ogasawara, Y. Takahashi, K. Kanbara, Y. Kubota, K. Yasohama and Y. Yasukochi, "Transient field losses in multifilamentary composite conductors carrying dc transport currents," *Cryogenics* vol. 20, Issue 4, 1980, pp. 216-222.

[23] P. Bruzzone, B. Stepanov, K. Sedlak, V. Corato, "A new test method of AC loss assessment for fusion conductors", *Fus. Eng. Des.*, vol. 146, 2019, pp. 928-931.